Lithosphere

Research Article

Dynamic Sealing Behavior of Sand Self-Juxtaposition Windows on a Trap-Bounding Fault in a Natural Gas Storage Site

Xiaoling Zhang,[1] **Xiaofei Fu** ⓘ**,**[1,2] **Yachun Wang,**[1] **Lingdong Meng** ⓘ**,**[1,2,3] **Ruishan Du,**[1,2] **Shuxin Hong,**[4,5] **Hongsong Yang,**[6] **Xiandi Fu,**[5] **Yabin Cheng,**[7] **Jian Li,**[7] **and Baishuang Zhang**[8]

[1]*School of Earth Sciences, Northeast Petroleum University, Daqing, Heilongjiang 163318, China*
[2]*Key Laboratory of Continental Shale Hydrocarbon Accumulation and Efficient Development, Ministry of Education, Northeast Petroleum University, Daqing, Heilongjiang 163318, China*
[3]*FAPS Energy Technology Ltd., Daqing, Heilongjiang 163318, China*
[4]*Daqing Oilfield Research Branch of Key Laboratory of Carbonate Reservoir, CNPC, Daqing, Heilongjiang 163712, China*
[5]*Exploration and Development Research Institute of Daqing Oilfield Company Ltd., Daqing, Heilongjiang 163712, China*
[6]*No. 3 Oil Production Plant of Daqing Oilfield Company Ltd., Daqing, Heilongjiang 163113, China*
[7]*Research Institute of Exploration and Development, Dagang Oilfield Company, Tianjin 300280, China*
[8]*Jia Jing Petroleum Engineering Technology Ltd., Daqing, Heilongjiang 163318, China*

Correspondence should be addressed to Lingdong Meng; lingdong.meng@hotmail.com

An understanding of across-fault seals is essential for planning an injection/production strategy for a fault-bounded gas storage site. In addition, it is more likely to permit lateral leakage for a fault with sand self-juxtaposition windows. This paper is aimed at identifying the dynamic sealing behaviors of a sand self-juxtaposition fault on the geological and gas injection timescales. Banzhongbei gas storage site, China, was taken as a target area, and fault seals and hydrocarbon distributions within the original reservoirs were studied. The results showed that across-fault pressure differences of 0.085~0.146 MPa (equivalent to 41.6~71.5 m oil-column and 27.0~46.4 m gas-column heights) were supported by sand self-juxtaposition windows on the B816 fault, and the resultant absolute permeability (5.97×10^{-2}~5.69×10^{-1} mD) of the fault was nearly 3~4 orders of magnitude lower than the average absolute permeability of reservoirs (1.16×10^2 mD). Gas composition contrasts, between the original and injection gas coupled with dynamic pressure monitoring data, indicated that lateral leakage occurred across sand self-juxtaposition windows under the condition of high across-fault pressure difference. However, the low-permeability fault showed strong negative influence on the efficiency of fluid flow in the model calculations and prolongs the timescales of pressure-difference decayed as much as 5 orders of magnitude relative to those of nonfault model calculations. These modeled dynamic sealing behaviors of sand self-juxtaposition windows may lead to a better understanding of the relative retardation of across-fault gas flow by weak sealing faults on the gas injection/production timescale.

1. Introduction

Reservoir self-juxtaposition windows occurring on trap-bounding faults are routinely regarded as sites of across-fault leakage [1, 2] or of little sealing capacity [3, 4] on the geologic timescale. This situation is likely to be true for faults developed in tight reservoirs owing to the occurrence of more permeable fractures within fault zones relative to host rocks, such as faults in volcanic rocks or tight sandstone [5, 6]. In porous sandstone, however, cataclasis is a common deformation process in the depth range of c. 1000-3000 m, resulting from mechanical shearing with grain comminution, reorganization, and denser packing [7]. Numerous scientific contributions confirm that cataclastic bands control the

amount of permeability reduction (one to six orders of magnitude) with respect to undeformed sandstone [7–19] in both extensional and contractional regimes [7, 20–23]. Cataclastic bands have a negative influence on fluid flow efficiency [24–27], in particular on two-phase flow [28]. Moreover, cataclasis-resultant deformation with higher capillary displacement pressure could support an approximately 20 m column height, and this may be ignored for exploration purposes [4, 29]. In extreme cases, fault core slip zones could possess up to a 75 m high column of hydrocarbons [30] or even a >140 m oil column, in which relatively higher theoretical sealing capacity may occur in contrast to a single deformation band, deformation band cluster, and slip-surface cataclasite [26]. The fluid flow retardation extent of deformation bands is particularly dependent upon their abundance and continuity in 3D space, as well as the petrophysical properties of the bands [24, 31]. The petrophysical properties of deformation bands generally present relatively low permeability and high capillary displacement pressure, which are controlled by cataclasis intensity, partly owing to the displacement [32] or strain magnitude [26, 33] and effective normal stress at the time of deformation [12, 34] under the same clay-content condition.

Hence, subseismic sand self-juxtaposition faults with fault core slip zones generally show higher cataclasis intensity and better continuity, which are likely to impede fluid flow to the same extent or to a larger extent than cataclastic bands due to larger displacement or larger strain [7, 35, 36]. Published studies on the petrophysical properties of deformation within sandstones are performed by means of field and laboratory measurements such as those cited above. However, their effects on fluid flow in an oil field still urge to be investigated.

This paper is aimed at identifying the dynamic sealing behaviors of a sand self-juxtaposition fault on the geological and gas injection timescales. Banzhongbei gas storage site (BGS), China, was taken as a target area, and fault seals and hydrocarbon distributions within the original reservoirs were studied. First, fault seals and hydrocarbon distributions within the original reservoirs were carried out to clarify the sealing capacity of the trap-bounding fault by using the hydrocarbon column height of original reservoirs, fault juxtaposition type, and densities of hydrocarbon and brine. Moreover, the across-fault fluid communication and the dynamic sealing behavior of the fault were investigated via analysis of production data including dynamic pressure monitoring data and the gas composition contrast between the original and injected gas. Finally, simplified model calculations were performed to quantify the influence of low-permeability sand self-juxtaposition windows on the timescale of the across-fault pressure-difference decay.

2. Geologic Setting

BGS is a turbidite hydrocarbon field of Oligocene age that contained fault-bounding gas condensate reservoirs put into production in 1974 and once depleted and became a gas storage site in 2003, acting as a swing supplier to meet the peak demand for natural gas for heating in Beijing, Tianjin,

and Hebei Province (Figure 1). Periods of gas injection and production are approximately 7 months (April to and October) and 5 months (November to next year March), respectively. In general, there is a one-month-long interval between gas injection and production for well maintenance. The multilayered reservoirs are Ban-II-1~4 sandstones (typical porosity approximately 18.3%, permeability 1.16×10^2 mD) with an original hydrostatic water gradient of 10.3 MPa/km and oil and gas densities of 826 kg/m^3 and 716 kg/m^3, respectively, which phase-state change has been considered in the condensate gas reservoir [37]. Overlying is a shale bed with a thickness of approximately 400 to 1600 m that provides an excellent cap seal (the vertical heterogeneity of the caprock and reservoir series is illustrated by the B12-24 well with a V_{shale} log in Figure 1).

BGS is located on the footwalls of two normal faults, namely, the ENE-WSW-trending Banqiao fault (BQF) and the NE-SW-trending B816 fault (Figure 1). The 814 Fault Block (814-FB) with two production layers Ban-II-1~2 is on the hanging wall of the B816 fault. Figure 1 illustrates that both the BGS and 814-FB are located on the footwall of BQF. According to the conclusion drawn by a former contribution Meng et al. [38, 39], BQF with throws of 140 to 3600 m leads to hydrocarbon-bearing reservoirs, completely juxtaposing caprock shale with little opportunity for gas seepage [40] and forming an extremely good lateral seal for both BGS and 814-FB. Additionally, the two traps have been integrated into one storage facility due to the high leakage possibility of the B816 fault with sand self-juxtaposition windows caused by a subseismic-scale throw of approximately 6 m at the crest of the trap-bounding segment. However, the exact sealing capacity of sand self-juxtaposition windows is still unclear and whether this sealing capacity influences on pressure communication across B816 fault during gas injection/ production periods is urge to explore.

3. Fault-Seal Analysis of the Original Hydrocarbon Trap

3.1. Original Hydrocarbon Distributions Within Fault Traps. Exploration-appraisal wells were set on BGS and 814-FB to clarify the spatial hydrocarbon distributions within the Ban-II-1~2 reservoirs (Figure 1). Fluid contacts of the original reservoirs including gas-oil contacts (GOCs) and oil-water contacts (OWCs) were well constrained by multiwell drilling data (Figure 2). BGS is filled to spill and that only a few meters of oil column are trapped (Figure 2). On the hanging wall of the B816 fault (814-FB), a much larger gas and oil columns are present in the Ban-II-1 reservoir, and only oil has been discovered in the Ban-II-2 reservoir. The trapped hydrocarbon columns in 814-FB have OWCs that are much shallower than the structural spill points of the two reservoirs. Thus, the hydrocarbon-bearing sand reservoirs on both sides of the B816 fault have different fluid contacts (Figure 2), although sand self-juxtaposition windows with more leakage possibility are confirmed to be present on the top of trap-bounding fault segments (Figure 1) [39].

It should be emphasized that the crosssection in Figure 2 illustrates only the juxtaposition types of the Ban-II-1
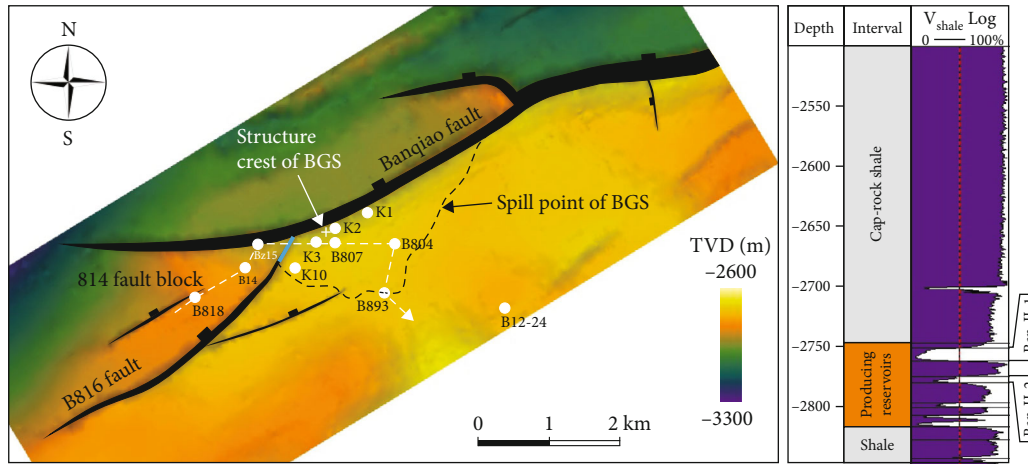
FIGURE 1: Locations of BGS and the 814 Fault Block and the vertical heterogeneity of the stratigraphy using the V_{shale} log from the B12-24 well. K1, K2, K3, and K10 are gas injection wells, and the others are exploration-appraisal wells, among which the Bz15 well was changed to a monitored well in 2014. The white dashed line represents the direction of the crosssection shown in Figure 2. The short blue line denotes the approximate position of the sand self-juxtaposition fault segments relative to depth range of 2715~2727 m and 2735~2747 m shown in Figure 4.
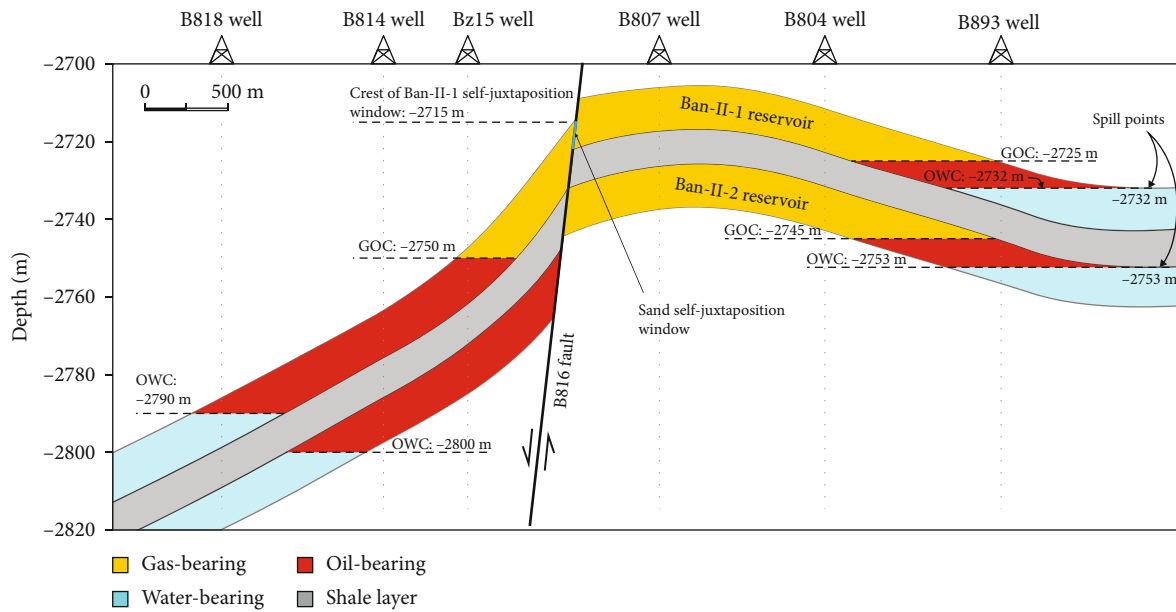

FIGURE 2: Crosssection (the white dash line located in Figure 1) through B816 fault with the approximately 6 m minimum throw of the Ban-II-1 reservoir highlighting the different fluid contacts across the sand self-juxtaposition window marked with a short blue line on B816. The depths of -2715 m and -2735 m annotated as the crest of the sand self-juxtaposition window are used as parameters in the height calculation for the self-juxtaposition window. Fluid contacts labeled with GOC and OWC are well constrained by exploration-appraisal wells. The upper and lower reservoirs denote the Ban-II-1 and Ban-II-2 sand layers bearing different fluid types. The colored legend for the gas-bearing, oil-bearing, and water-bearing parts within reservoirs and the shale layer is shown in the lower right corner.

reservoir under the condition of the 6 m throw of the Ban-II-1 top rather than describing that of the Ban-II-2 reservoir in the same circumstance because the sand self-juxtaposition windows of the two reservoirs cannot be expressed in one vertical crosssection due to the difference in apparent layer thicknesses caused by layer rotation. The crests of intersections between the B816 fault and the two hanging wall reservoirs tops, which represent the crests of two self-

juxtaposition windows, are confirmed to be approximately -2715 m and -2735 m for the Ban-II-1 and Ban-II-2 reservoirs, respectively, by 3D seismic data and drilling data. These depths are used to calculate the depth ranges of the two self-juxtaposition windows in the next section.

3.2. Geohistorical Sealing Capacity of Sand Self-Juxtaposition Windows. Due to an absence of sufficiently detailed
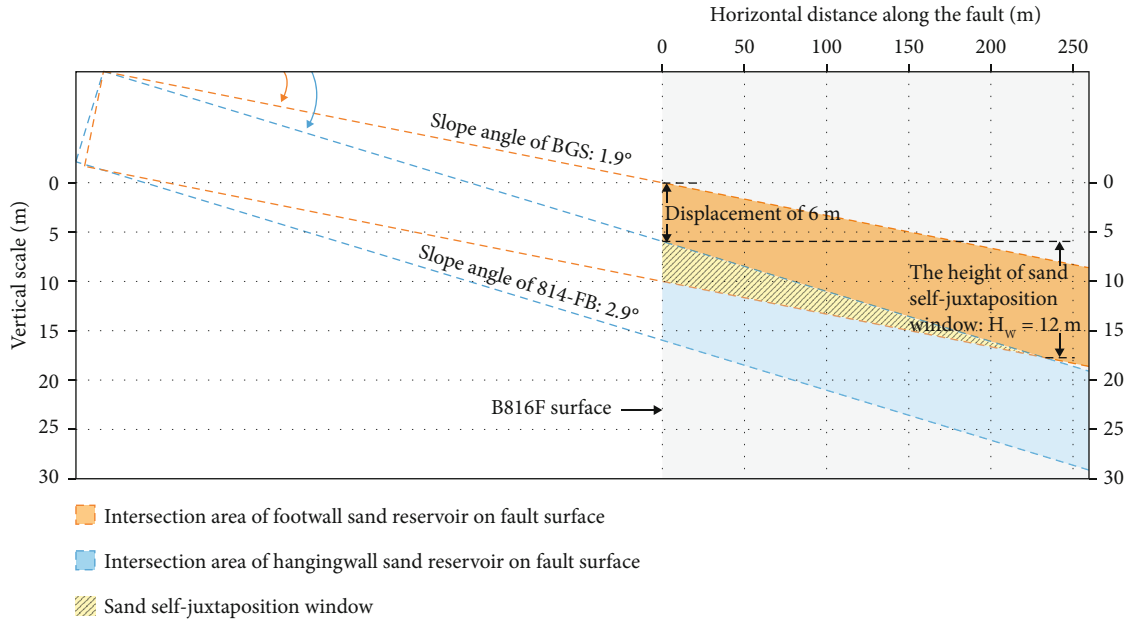
FIGURE 3: The height calculation ($H_w = 12$ m) for the sand self-juxtaposition window (the obtuse triangle with yellow shading) on the B816 fault surface using the average slope angles of the footwall (1.9°) and hanging wall (2.9°) sand reservoirs along the B816 fault surface (gray zone) coupled with vertical fault displacement of 6 m and average reservoir thickness of 10 m. The abscissa denotes the along-fault horizontal distance to the top of the trap-bounding segment. The vertical axis is a relative scale to show the displacement, reservoir thickness, and calculated height of the sand self-juxtaposition window. Yellow and blue arrows in the upper part show the layer rotation, and colored zones are interpreted using the legend in the lower left corner.

measurements of a sand self-juxtaposition fault zone, an empirical approach, fault-seal calibration by geohistory, is used to confirm the minimum pressure difference that could be supported by a fault. Detailed descriptions of how this methodology could be implemented to determine fault-seal capacity in a routine faulted reservoir scenario [41, 42]. In this case, confirming the depth ranges of sand self-juxtaposition windows on the B816 fault is important to quantify how much across-fault pressure difference could be supported by these windows. Owing to the limit of seismic resolution, robust seismic interpretation of horizon data near the faults is lacking. Thus, the average slope angles of 814-FB (2.9°) and BGS (1.9°) along the B816 fault are used to calculate the heights of the sand self-juxtaposition windows of the two producing reservoirs (Figure 3). By combining this information with the B816 fault throws of 6 m near the crests of both traps and average reservoir thickness of 10 m, a sand self-juxtaposition window with a 12 m depth range was calculated, which is shown as the overlap zone of the footwall and hanging wall sand reservoirs on the B816 fault (Figure 3). Thus, the depth ranges of sand self-juxtaposition windows for Ban-II-1 and Ban-II-2 are calculated as -2715 to -2727 m and -2735 to -2747 m, respectively, according to the aforementioned crest depths. Then, a different pressure profile in each of the two traps can be constructed based on the fluid contacts coupled with the hydrostatic pressure gradient and the hydrocarbon densities of the original reservoirs (Figure 4). In light of this information, the oil and gas pressures on both sides of the B816 fault can be obtained and expressed by the following equations:

$$P_{\text{oil}(814-\text{FB})}^{\text{Ban}-\text{II}-1} = \rho_{\text{oil}}gD \times 10^{-6} + 5.692,$$

$$P_{\text{gas}(814-\text{FB})}^{\text{Ban}-\text{II}-1} = \rho_{\text{gas}}gD \times 10^{-6} + 8.717,$$

$$P_{\text{oil}(\text{BGS})}^{\text{Ban}-\text{II}-1} = \rho_{\text{oil}}gD \times 10^{-6} + 5.573,$$

$$P_{\text{gas}(\text{BGS})}^{\text{Ban}-\text{II}-1} = \rho_{\text{gas}}gD \times 10^{-6} + 8.571, \qquad (1)$$

$$P_{\text{oil}(814-\text{FB})}^{\text{Ban}-\text{II}-2} = \rho_{\text{oil}}gD \times 10^{-6} + 5.712,$$

$$P_{\text{oil}(\text{BGS})}^{\text{Ban}-\text{II}-2} = \rho_{\text{oil}}gD \times 10^{-6} + 5.616,$$

$$P_{\text{gas}(\text{BGS})}^{\text{Ban}-\text{II}-2} = \rho_{\text{gas}}gD \times 10^{-6} + 8.636,$$

where $P_{\beta(\gamma)}^{\alpha}$ in MPa represents β (fluid type) pressure of α (sand reservoir) layer in γ (trap name) trap, such as $P_{\text{oil}(\text{BGS})}^{\text{Ban}-\text{II}-1}$ means the oil pressure of the Ban-II-1 reservoir in BGS. ρ_{oil} and ρ_{gas} denote an oil density of 826 kg/m³ and a gas density of 716 kg/m³, respectively. The g value of 10 m/s² is the acceleration of gravity. D is the true vertical depth in meters. Thus, the across-fault pressure difference (AFPD) in the depth ranges of the self-juxtaposition windows on the fault surface can easily be determined (Table 1).

The fluid contact differences across the B816 fault imply that sand self-juxtaposition windows have some sealing capacity. If we assume that the sand self-juxtaposition windows on the B816 fault have reached their upper limit of sealing capacity, then the calibrated AFPD of 0.085~0.146 MPa (see Table 1) can be used as an estimate of the capillary displacement pressure of the sand self-juxtaposition windows. Then, the corresponding maximum sustainable oil and gas
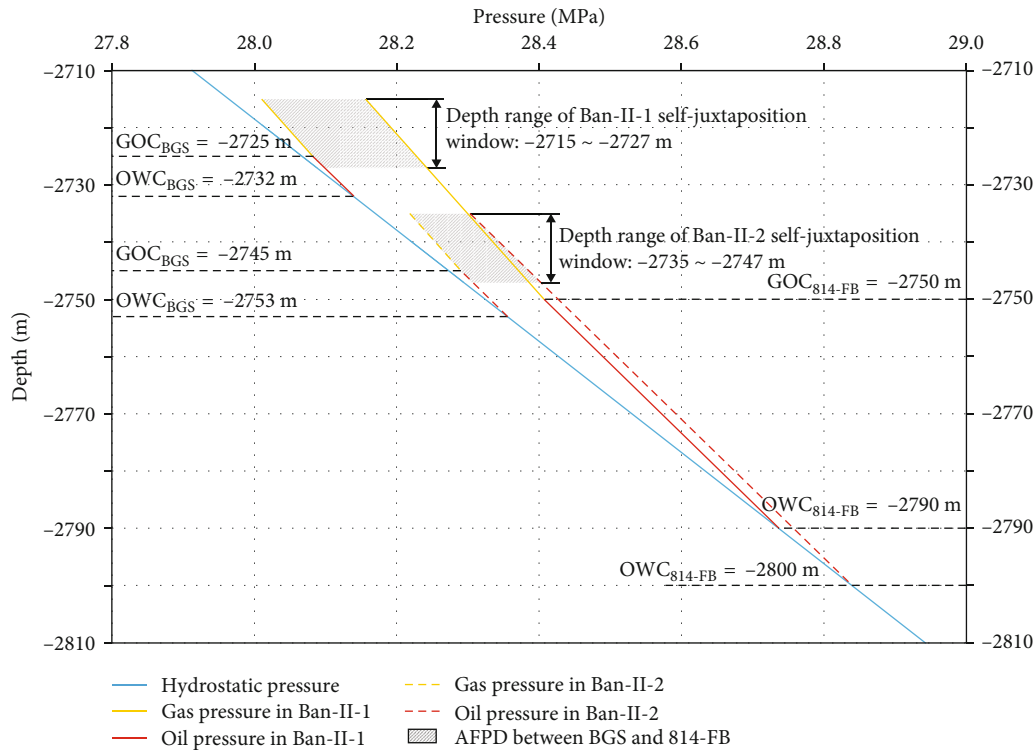
FIGURE 4: Pressure profile showing the fluid contacts (GOC and OWC) in the two producing sand reservoirs on 814-FB and BGS. The oblique lines represent the hydrostatic pressure gradient (blue line) and hydrocarbon pressure gradients in the Ban-II-1 reservoir (red and yellow solid lines) and Ban-II-2 reservoir (red and yellow dashed lines). The horizontal distance within the gray shaded regions in the self-juxtaposition depth ranges denote AFPD between BGS and 814-FB.

column heights of up to 71.5 m and 46.4 m, respectively, can be calculated according to the fluid densities of the original reservoirs (Table 1). Moreover, according to the correlations between capillary displacement pressure (P_d) and permeability described by Hildenbrand et al., AFPD can be further converted into fault zone effective permeability (k_{eff}) for the gas-water system and absolute permeability (k_{abs}) for gas (Equations (2) and (3)) [43].

$$\log (P_d) = -0.8112 \times \log (k_{abs}) + 1.1549, \quad (2)$$

$$\log (P_d) = -0.3763 \times \log (k_{eff}) + 0.218, \quad (3)$$

where P_d is the capillary displacement pressure for the gas-water system in MPa, which is replaced by AFPD for calculating the fault zone permeability. k_{abs} and k_{eff} represent the absolute permeability (10^{-3} mD) for gas and the effective permeability for the gas-water system, respectively. We use the correlations between capillary displacement pressure (P_d) and permeability (K_{eff} and K_{abs}) established from CH_4 experiments [43] for two principle reasons listed below.

(1) The injection gas permeability of a fault zone may be mainly dependent on the permeability for CH_4, because CH_4 is the dominant gas component with molar concentrations of >90% of the total injection gas (Table 2). Thus, the permeability calculated from $P_d - K_{eff}$ to $P_d - K_{abs}$ correlations for CH_4 cited above could be the best-fit results to describe the retardation of fluid flow by faults

(2) The AFPD used to represent the fault zone P_d ranges from 0.08 to 0.15 MPa, which is in the P_d range of 0.06~3.65 MPa for CH_4 as described by Hildenbrand et al. [43]. Thus, using the $P_d - K_{eff}$ and $P_d - K_{abs}$ correlations to invert the fault zone permeabilities is likely reasonable

The resultant calculated permeability ranges of the two reservoirs are compiled in Table 1. The absolute permeability is calculated for investigating the effects of the sand self-juxtaposition windows on single-phase gas flow across a fault, as discussed below. The absolute permeabilities of Ban-II-1 and Ban-II-2 are 5.97×10^{-2}~6.36×10^{-2} mD and 3.42×10^{-1}~5.69×10^{-1} mD, respectively, which are approximately 3~4 orders of magnitude lower than that of the reservoirs (1.16×10^2 mD). This estimate of permeability reduction, dominantly controlled by cataclasis within the core zone of faulted porous sandstone, is approximately consistent with numerous experimental results for cataclastic bands [12, 13, 19, 24, 44]. However, the possibility that permeability reduction is caused by localized quartz cementation or shale/clay smear resulting from extremely thin shale/clay layers cannot be ruled out, because the original reservoir temperature of 85°C is close to the critical condition for quartz pressure solution (>90°C), and proving

TABLE 1: Calibrated AFPD and calculated fault zone permeability of sand self-juxtaposition windows.

Producing layer	Depth range of self-juxtaposition window (m)	Calibrated AFPD (MPa)	Sustainable oil-column height (m)	Sustainable gas-column height (m)	Absolute permeability k_{abs} (mD)	Effective permeability k_{eff} (mD)
Ban-II-1	-2715	0.144	70.4	45.7	5.97×10^{-2}	2.10×10^{-4}
	—	—	—	—	—	—
	-2727	0.146	71.5	46.4	6.36×10^{-2}	2.19×10^{-4}
Ban-II-2	-2735	0.085	41.6	27.0	3.42×10^{-1}	6.74×10^{-4}
	—	—	—	—	—	—
	-2747	0.096	47.0	37.5	5.69×10^{-1}	9.45×10^{-4}

Note: oil and gas densities $0f$ 826 kg/m³ and f 716 kg/m³, respectively, are used to calculate the sustainable oil- and gas-column heights of the fault. The correlations between "calibrated AFPD" and "absolute and effective permeabilities" are presented in form of Equations (2) and (3) described by Hildenbrand et al. in 2004.

TABLE 2: Gas composition contrast between the original, the monitored gas from the Bz15 well, and the injection gas.

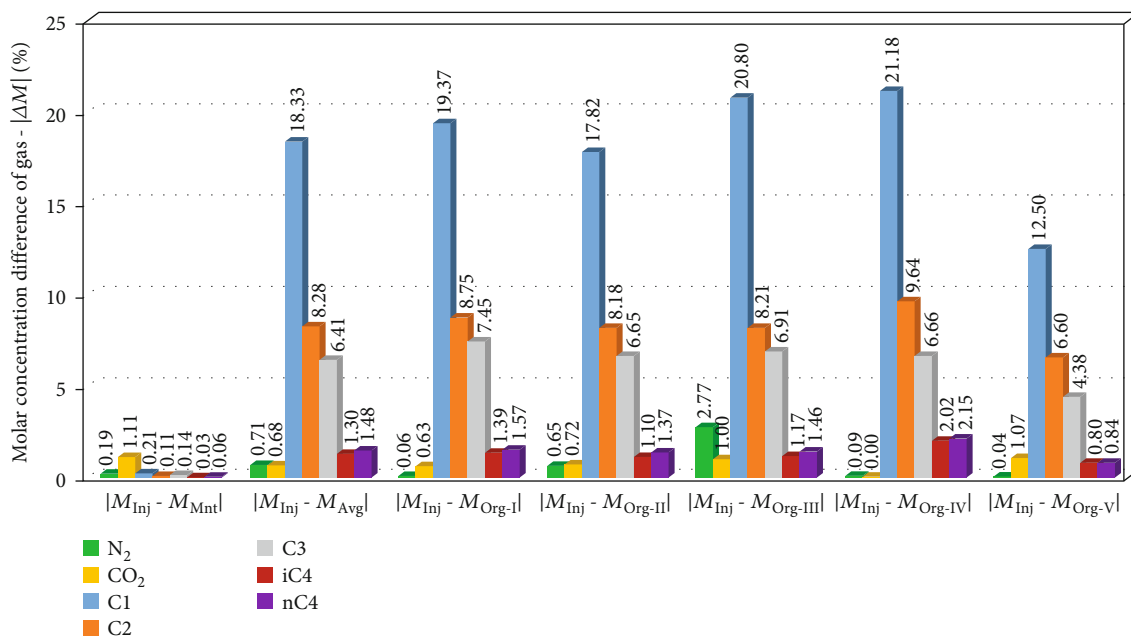| Gas composition | The molar concentration of original gas in the early stage of exploration (%) | | | | | The average molar concentration of original gas (%) | The monitored molar concentration of gas after injection in May 2014 (%) | The molar concentration of injection gas (%) |
	M_{Org-I}	M_{Org-II}	$M_{Org-III}$	M_{Org-IV}	M_{Org-V}	M_{Avg}	M_{Mnt}	M_{Inj}
N_2	0.72	1.31	3.43	0.75	0.62	1.37	0.85	0.66
CO_2	0.63	0.72	1.00	0.00	1.07	0.68	1.11	0.00
C1	73.61	75.16	72.18	71.80	80.48	74.65	92.77	92.98
C2	12.50	11.93	11.96	13.39	10.35	12.03	3.86	3.75
C3	8.13	7.33	7.59	7.34	5.06	7.09	0.82	0.68
iC4	1.51	1.22	1.29	2.14	0.92	1.42	0.15	0.12
nC4	1.69	1.49	1.58	2.27	0.96	1.60	0.18	0.12

FIGURE 5: Molar concentration differences for each gas component between injection gas (M_{Inj}), monitored gas (M_{Mnt}), and original gas (M_{Avg}, M_{Org-I} to M_{Org-V}). M_{Org-I} to M_{Org-V} are the original gas components resulting from five production records during the early stage of hydrocarbon exploration. M_{Avg} represents the average molar concentration of the original gas components.

whether thin shale/clay layers are present is difficult when depending only on V_{shale} logging without the help of core samples. The estimate AFPD and permeability suggest that the sealing behavior of sand self-juxtaposition windows may not be completely neglected on geohistoric or production timescales in some cases.

4. Fault-Seal Behavior during Gas Injection

4.1. Across-Fault Gas Composition and Pressure Differences. To clarify the contributions of the low-permeability sand self-juxtaposition windows of the B816 fault to fluid flow, data from the Bz15 well located in 814-FB was analyzed. The Bz15 well was a production well from its inception and then became a monitoring well in 2014 for the purpose of gas composition and dynamic pressure monitoring during gas injection/production in BGS. Accordingly, the analysis of whether lateral leakage across the fault occurred during gas injection can be carried out using monitored gas components and pressure variations in B814-FB. Theoretically, if identical gas compositions or pressure trends are observed in injection wells and the monitored well, this would indicate a leaky fault; conversely, the fault is sealing at the time scale of observation.

In the case of the main gas components C1, C2, and C3, the original condensate gas has molar concentrations of C1, C2, and C3 ranging from 71.80~80.48%, 10.35~12.50%, and 5.06~8.13%, respectively, as shown in Table 2. By contrast, the three components within the injection gas are 92.98%, 3.75%, and 0.68%, respectively. This comparison is taken further by using the absolute differences in the molar concentration of each component ($|\Delta M|$) between the injection gas from K1, K3, K5, and K10 located in Figure 1 (M_{Inj}), the

monitored gas (M_{Mnt}), and the original gas including five gas recovery records (M_{Org-I} to M_{Org-V}) combined with their average value (M_{Avg}) from the Bz15 well to describe the change in each gas component that occurred in 814-FB after injection into BGS (Table 2). The gas component differences for C1, C2, and C3 between original and monitored gas can be seen in Figure 5, as well as the differences in N_2, CO_2, and i/nC4. Obviously, from the negligible difference between the injection and the monitored gas, the injection gas has been broken through the sand self-juxtaposition windows of the B816 fault and been monitored by the Bz15 well.

Moreover, during the stage of gas injection in BGS, the bottom-hole pressure in the Bz15 well showed a dramatic increase after it was converted from a production well to a monitoring well on 24 June 2014 (see the black dash line in Figure 6). The bottom-hole pressure difference between the K3 well (the nearest well to the Bz15 well) and the Bz15 well was taken as an example. This difference decreased sharply from 7.81 MPa to 2.82 MPa (one to two orders of magnitude higher than the calibrated AFPD of 0.085~0.146 MPa) in one day caused by the end of hydrocarbon recovery and then continued to decrease gradually to 1.08 MPa by 14 July 2014. The period of 24 June 2014 to 14 July 2014 is regarded as a stage of pressure-difference decay mainly caused by the low-permeability of the B816 fault. After this stage, the variation in the pressure difference remained in a relatively small range of 1.00~1.72 MPa owing to both the pressure-difference decay across the fault and the continuous gas injection in the form of relatively constant injection pressure and rate. The process of the slow pressure-difference decrease shows the positive contribution of the pressure supply from gas injection in BGS. Additionally, pressure vs. time was following a rather similar trend of pressure changes in other injection wells (K1, K2,
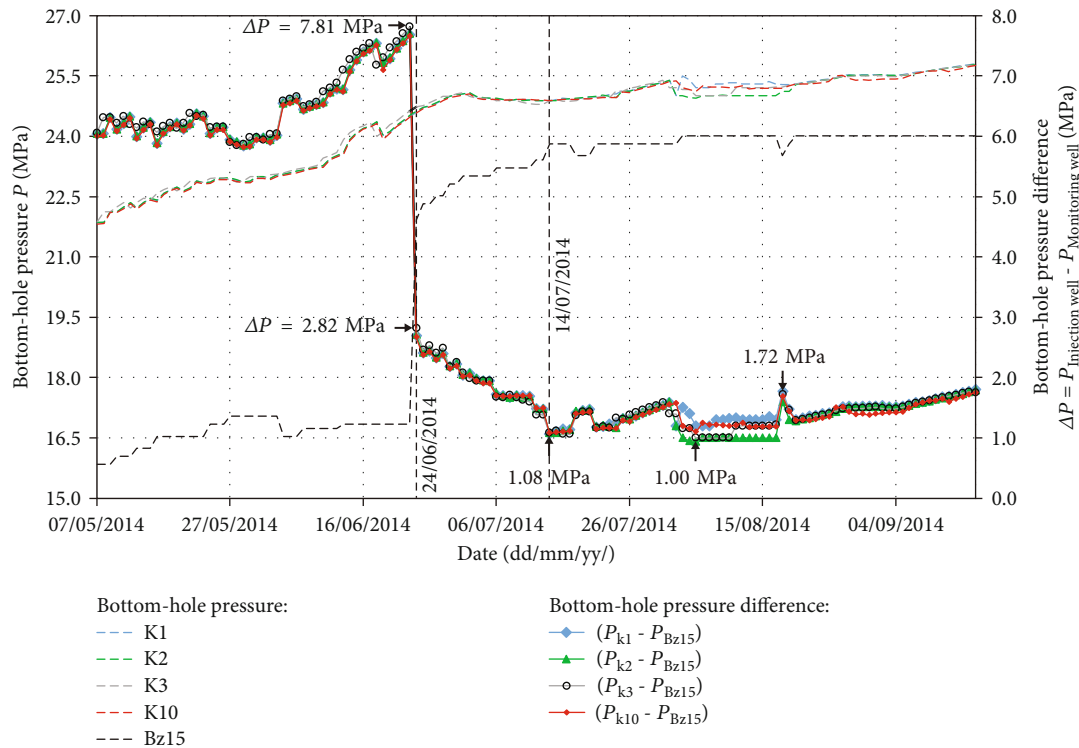
FIGURE 6: Bottom-hole pressure variations in the monitoring well (Bz15) and injection wells (K3-1/2/3/10) according to the date. The left vertical axis refers to the bottom-hole pressure. The right axis denotes the bottom-hole pressure difference between injection wells and the monitoring well.

K3, and K10 wells) besides the B816 fault both before 24 June 2014 and after 14 July 2014 (Figure 6; see Figure 1 for well locations).

This observation combined with the monitored gas composition results provides robust evidence that sand self-juxtaposition windows with weak sealing capacity can allow fluid communication under conditions of high AFPD caused by gas injection on one side of the fault. Nevertheless, bottom-hole pressure differences of 1.0 to 1.72 MPa between the Bz15 well and K3 well remained after 14 July 2014 during gas injection (Figure 6), which may suggest that the sand self-juxtaposition windows still play a role in controlling the timescale of pressure-difference decay across a fault. This demonstrates that in the case of this field example, identifying the fault sealing behaviors on the gas injection/production timescale is essential.

4.2. Dynamic Sealing Behavior of Sand Self-Juxtaposition Windows. For characterizing the dynamic sealing behaviors of sand self-juxtaposition windows in this section, four simplified model calculations are presented of the likely timescales of pressure-difference decay across faults following the introduction of gas injection pressure. The calculations are divided into groups A and B based on flow distances (L) of 600 m and 1600 m, respectively (Figure 7(a)). The flow distances of groups A and B are ideally determined by the relative straight-line distances from injection well K10 to monitoring Bz15 and from the K1 well to the Bz15 well, allowing an analysis under the condition of realistic flow distance. Each group includes a nonfault and a low-permeability

fault model calculation with identical reservoir thickness (T) in order to highlight and quantify the influence of the low-permeability sand self-juxtaposition windows on the timescale of pressure-difference decay across a fault. Although the fluid flow within a realistic model is much more complex than the ones shown above, this work emphasis centers on the difference between the non-fault model and the low-permeability fault model.

Notably, the capillary displacement pressures of the sand self-juxtaposition windows in the B816 fault have been exceeded since the operation of gas storage, and the fault zone is likely saturated by injection gas after more than ten years of gas injection/production. Thus, the fault zone flow behavior should be a function of the permeability. In light of this relation, we use the absolute permeability of gas (K_{abs}) shown in Table 1 in the model calculations assuming a gas-saturated reservoir and fault zone. The calculation is based on a diffusion equation for single-phase flow and models the decay of excess pressure after the introduction of a pressure pulse (gas injection) or depletion (due to production) on one side of the fault. The correlation between the normalized AFPD ($\Delta\text{AFPD}_{\text{pot}(t)}/\Delta\text{AFPD}_{\text{pot}(0)}$) and the timescale of the pressure-difference decay (t) can be expressed as follows for identical reservoir thicknesses and widths on both sides of the fault [45]:

$$\frac{\Delta\text{AFPD}_{\text{pot}(t)}}{\Delta\text{AFPD}_{\text{pot}(0)}} = e^{-2kt/\mu\beta_f x\varphi L}, \tag{4}$$
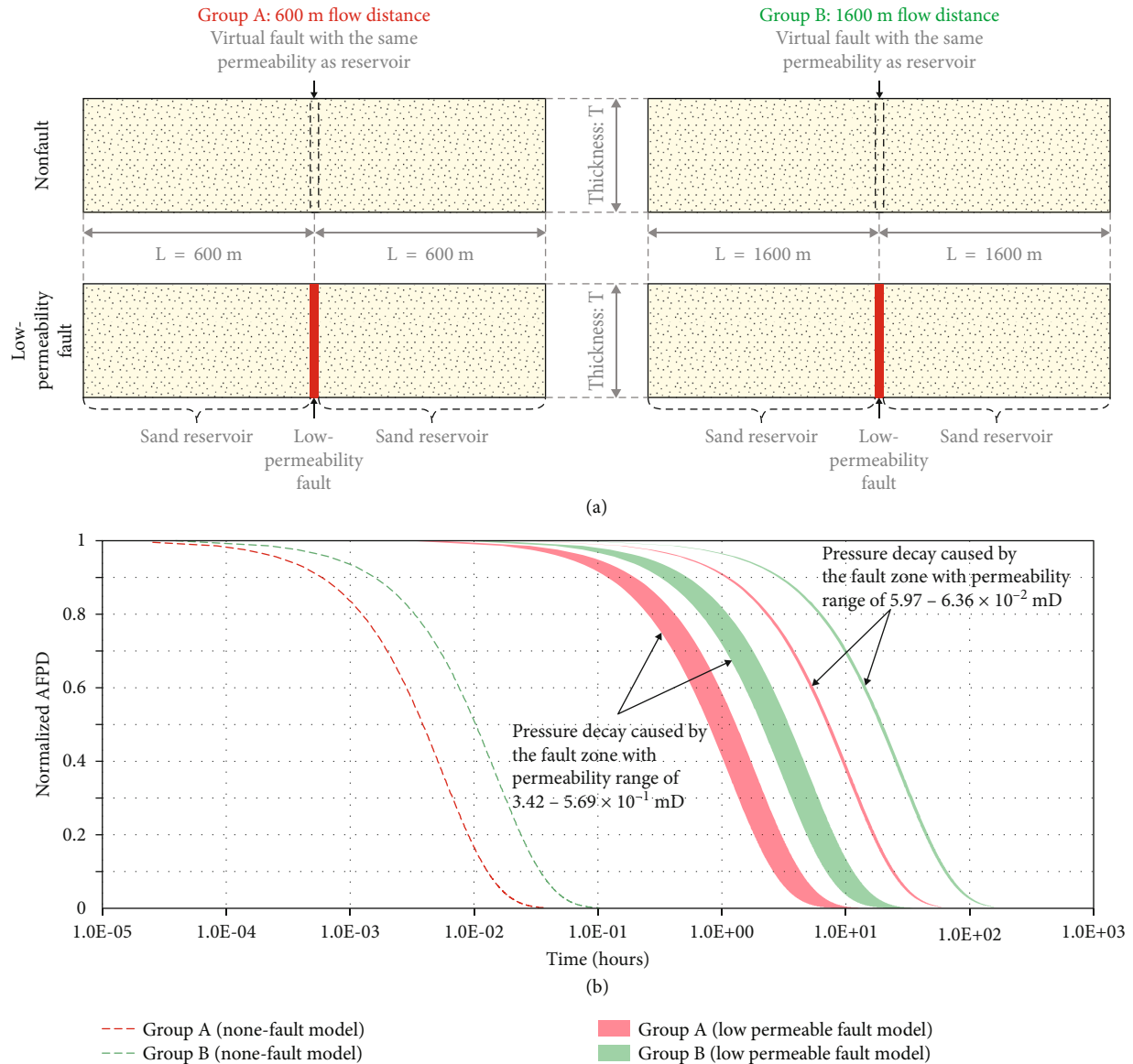
FIGURE 7: (a) Model calculations of the timescales of across-fault pressure decay. Both groups A and B include a nonfault model calculation and another with a low-permeability fault set in the center. The flow distances on one side of the fault in the two model calculations with identical reservoir thickness (T) are 600 m and 1600 m. The permeability of the low-permeability fault with a fault core thickness of 0.1 m is 2.85 to 5.55×10^{-4} mD. In the nonfault models, virtual faults are set with identical fault zone thicknesses using a permeability of 1.16×10^{2} mD. (b) Results of the model calculations for timescales of pressure dissipation across a fault as functions of fault permeability from four models. Yellow dashed lines are the results of nonfault model calculations in groups A and B. Blue and red dashed lines represent the results from the minimum and maximum fault zone permeability in both groups, respectively.

where t is the time elapsed since the end of the pressure pulse and $\Delta AFPD_{pot}$ indicates the AFPD at identical depths (or the pressure potential difference) for time t. Initially, at time $t = 0$, k is the permeability in mD of the central fault core zone with thickness of x in meters. Further, μ denotes the fluid viscosity in Pa·s, β_f is the fluid compressibility, φ is the porosity, and L is the length of each of the two sides of the fault in the model calculations (Figure 7(a)).

Based on the correlations between gas viscosity, density, temperature, and pressure [46, 47], the gas viscosity is defined as 2.3×10^{-5} Pa · s at a gas density of 700 kg/m^3, temperature of 85°C and reservoir pressure of 25 MPa. The gas compressibility is confirmed to be 1.72×10^{-8} Pa^{-1} under the same geologic conditions. The thickness of the fault core zone, which increases approximately with increasing fault throw or displacement in all rock types [48–52], is simplified as one-sixtieth of the fault throw according to the positive relationship used by Wibberley et al. [45]. Then, this value can be confirmed to be 0.1 m, resulting from the minimum throw of 6 m in the model calculations. Considering the gas-saturated reservoir and the fault zone, the absolute permeabilities of the sand self-juxtaposition windows in Ban-II-1 ($5.97 \times 10^{-2} \sim 6.36 \times 10^{-2}$ mD) and Ban-II-2 ($3.42 \times 10^{-1} \sim 5.69 \times 10^{-1}$ mD) compiled in Table 1 are used to describe

the retardation of gas flow by faults. In the nonfault model calculation, a virtual fault with the same permeability as the reservoir is set instead of the fault zone with an identical thickness in the low-permeability fault model calculations.

Results from the low-permeability fault model calculation in group A show that 10 s of hours pressure-difference decay is observed across the 600 m long flowing distance when nearly 100% ΔAFPD dissipation occurs (solid lines filled with red color in Figure 7(b)). By contrast, approximately <150 hours pressure-difference decay is observed in the low-permeability fault model calculation in group B (solid lines filled with green color in Figure 7(b)). These results indicate that long-distance flow can undoubtedly prolong pressure-difference decay under the same fault-setting conditions, even when the reservoir permeability is much higher than that of the fault. Although a low-permeability fault within the model calculations can cause a timescale increment for pressure-difference decay of approximately 3 orders of magnitude with respect to the nonfault model calculation in both groups, the pressure-difference decay dissipates in less than 150 s of hours (ca. 6 days) in the models, which explained the 20-day-long period of pressure-difference decay (from 24 June to 14 July) observed in the field. As mentioned above, the interval between the gas injection and production periods for the storage facility is up to one month, which is long enough for dissipation of the pressure difference caused by gas injection in BGS. Thus, a 20-day-long period of pressure-difference decay appears to be negligible on the timescale of an entire cycle of gas injection and production for the storage facility.

However, it should be emphasized that the different fluid flow rates on the two sides of a fault caused by low-permeability sand self-juxtaposition windows play a paramount role in the realistic efficiency of gas injection/production. Taking the gas injection process as an example, the gas is likely to flow towards the spill point through the higher-permeability reservoirs with higher fluid flow rates relative to those across a fault, which may result in a large amount of gas escaping rather than being stored in the trap on the other side of the fault.

Thus, the permeability of a sand self-juxtaposition trap-bounding fault, even for a subseismic fault with a throw of several meters, may have an obvious influence on gas flow efficiency. It needs to be considered separately in the fluid flow simulation to help the gas storage to operate in a more efficient way, rather than to be simplified as a leakage medium with an empirical permeability value in traditional way [1]. The questions that remain include (1) should injection/production wells be placed on the hanging wall of B816 fault? and (2) what is a reasonable upper limit of gas injection pressure or rate?

5. Discussion

5.1. Uncertainties.
It is difficult to determine the dynamic sealing behaviors of subseismic faults, owing to the requirement of more precise data, such as fault displacement, reservoir thickness, fluid contacts, and fault properties.

Fault displacement mapping can lead to more inaccurate reservoir juxtapositions in a situation of lower seismic resolution, in particular, for a subseismic fault throws with a displacement similar to that of the reservoir thickness. Nevertheless, wells drilled through a fault can facilitate the constraint of displacement depending upon their repeated sections (reverse faults) or missing sections (normal faults) at the fault cut compared with nearby wells due to few lithology changes and complete stratigraphic sequences [53].

The reservoir thickness and the original fluid contacts are poorly defined and require better constrained drilling or well-logging data. Wells for determining reservoir thickness near the trap-bounding fault may be much more helpful to confirm the location of the intersection lines between reservoirs and trap-bounding faults. Similarly, wells drilled through or close to fluid contacts are necessary to provide robust evidence of original fluid contact locations.

Fluid properties including density, viscosity, and compressibility not only affect estimates of the original AFPD and calculated permeability but also have a significant influence on the further fluid flow simulation. Therefore, care must be taken to validate the dynamic sealing behaviors of a subseismic fault owing to uncertainties from the seismic resolution, well-logging data, and fluid properties from laboratory-based analyses or empirical equations.

5.2. Complexities.
The simplified ideal model assumptions in this workflow are used only to identify the effect of low-permeability sand self-juxtaposition windows in the timescale of pressure-difference decay across faults. Under complex realistic conditions, several other factors in addition to the fault sealing capacity potentially affect the timescale for pressure dissipation.

A case study shows that faults of offset <10 m have only 2 orders of magnitude permeability reduction in the fault core, and 1 order in the damage zone in shallow depth of <1000 m [10]. In this case, the fault zone absolute permeability of $5.97 \times 10^{-2} \sim 5.69 \times 10^{-1}$ mD is 3~4 orders of magnitude lower than the average absolute permeability of 1.16×10^2 mD in the depth of >2700 m. The higher permeability reduction, in this paper relative to the case study mentioned above, may be caused by a combined contribution of the fault core and damage zone, or/and the deeper depth with stronger cataclasis.

The area of the sand self-juxtaposition windows on the fault surface was shown in Figure 4. The area is very small corresponding to the crosssectional area of the reservoir cut by B816 fault. This implies that only an extremely small leakage window, relative to the whole area of the fault cut crosssection of the reservoir, allows across-fault gas flow within a single sand reservoir. Thus, the limited sand-sand juxtaposition window reduces the efficiency of gas flowing from BGS to 814-FB to a great extent.

The slope angles are different between BGS and 814-FB combined with the shapes of the two fault-bounding traps and cause the reservoir area of BGS to be much larger than that of 814-FB for a given contour line. Moreover, the spill point for BGS (trap height~30 m) is much shallower than that of 814-FB with a trap height of more than 100 m (see

Figure 2). Both cases lead to distinct boundary conditions which may be totally different from those in the ideal model calculations.

The final factor is dominantly caused by the heterogeneous petrophysical properties of reservoirs. The tops of Ban-II-1 and Ban-II-2 drilled through the Bz15 well are lower than the spill points of the two layers in BGS (Figure 2). As gas injection proceeds in BGS, the monitored gas in the Bz15 well indicates that the gas has likely reached the spill points of the two production layers of BGS; however, the realistic injection volume is still under the requirement of the designed gas injection volume at this moment. These data imply that high-pressure gas injection leads gas to flow preferentially in high-permeability paths present in turbidite sediments rather than homogeneously in reservoirs. Thus, the heterogeneity of reservoir permeability is another significant issue that needs to be considered in the fluid flow simulation [54].

Therefore, a more refined fluid flow simulation needs to be incorporated into planning an efficient gas injection/production strategy under realistic complex conditions considering the dynamic fault sealing behaviors, boundary conditions, heterogeneous petrophysical properties of reservoirs, etc.

6. Conclusions

This paper is aimed at identifying the dynamic sealing behaviors of a sand self-juxtaposition fault on the geological and gas injection timescales. Banzhongbei gas storage site, China, was taken as a target area, and fault seals and hydrocarbon distributions within the original reservoirs were studied. These modeled dynamic sealing behaviors of sand self-juxtaposition windows may lead to a better understanding of the relative retardation of across-fault gas flow by weak sealing faults on the gas injection/production timescale.

(1) Subseismic-scale sand self-juxtaposition windows on the B816 fault are important on the geohistoric timescale, with calibrated sealing capacities of 0.085 to 0.146 MPa. The maximum oil- and gas-column heights can be up to 71.5 m and 46.4 m, respectively, which could be a potential exploration target if the trap area is large enough

(2) The fault zone absolute permeability of 5.97×10^{-2} ~5.69×10^{-1} mD resulting from the calibrated AFPD is approximately 3~4 orders of magnitude lower than the average absolute permeability of 1.16×10^2 mD. It indicates that subseismic faulting within sandstone can play a significant role in permeability reduction at the depth of the case study. Thus, the permeability of a sand self-juxtaposition trap-bounding fault must be considered in fluid flow simulations. In this case, a gas storage site can operate in the efficient way

(3) Gas composition and dynamic pressure monitoring results suggest that the sealing capacity of a sand self-juxtaposition fault cannot significantly impede across-fault gas flow on the production timescale.

It is because that the high AFPD caused by gas injection/production may be 10 s to 100 s of times higher than what is likely to be supported by a weak sealing fault

Data Availability

Please contact the corresponding author to ask for related data, if any reader is interested in this research.

Conflicts of Interest

We declare that we have no conflicts of interest to this work.

Acknowledgments

References

[1] U. S. Allan, "Model for hydrocarbon migration and entrapment within faulted structures," *AAPG Bulletin*, vol. 73, pp. 803–811, 1989.

[2] W. R. James, L. H. Fairchild, G. P. Nakayama, S. J. Hippler, and P. J. Vrolijk, "Fault-seal analysis using a stochastic multifault approach," *AAPG Bulletin*, vol. 88, no. 7, pp. 885–904, 2004.

[3] R. B. Færseth, E. Johnsen, and S. Sperrevik, "Methodology for risking fault seal capacity: implications of fault zone architecture," *AAPG Bulletin*, vol. 91, no. 9, pp. 1231–1246, 2007.

[4] R. G. Gibson, "Fault-zone seals in siliciclastic strata of the Columbus Basin, offshore Trinidad," *AAPG Bulletin*, vol. 78, pp. 1372–1385, 1994.

[5] L. Meng, X. Fu, Y. Wang et al., "Internal structure and sealing properties of the volcanic fault zones in Xujiaweizi fault depression, Songliao Basin, China," *Petroleum Exploration and Development*, vol. 41, no. 2, pp. 165–174, 2014.

[6] F. U. Xiaofei, X. Shang, and L. Meng, "Internal structure of fault zone and oil/gas reservior in low-porosity rock," *Journal of Central South University*, vol. 44, pp. 2428–2438, 2013.

[7] G. Ballas, H. Fossen, and R. Soliva, "Factors controlling permeability of cataclastic deformation bands and faults in porous sandstone reservoirs," *Journal of Structural Geology*, vol. 76, pp. 1–21, 2015.

[8] S. Alkhasli, G. Zeynalov, and A. Shahtakhtinskiy, "Quantifying occurrence of deformation bands in sandstone as a function of structural and petrophysical factors and their impact on reservoir quality: an example from outcrop analog of productive series (Pliocene), south Caspian Basin," *Journal of Petroleum Exploration and Production Technology*, vol. 12, no. 7, pp. 1977–1995, 2022.

[9] M. Antonellini and A. Aydin, "Effect of faulting on fluid flow in porous sandstones: petrophysical properties," *AAPG Bulletin*, vol. 78, pp. 355–377, 1994.

[10] F. Balsamo and F. Storti, "Grain size and permeability evolution of soft-sediment extensional sub-seismic and seismic fault zones in high-porosity sediments from the Crotone basin, southern Apennines, Italy," *Marine and Petroleum Geology*, vol. 27, no. 4, pp. 822–837, 2010.

[11] F. Balsamo and F. Storti, "Size-dependent comminution, tectonic mixing, and sealing behavior of a "structurally oversimplified" fault zone in poorly lithified sands: evidence for a coseismic rupture?," *Geological Society of America Bulletin*, vol. 123, no. 3-4, pp. 601–619, 2011.

[12] Q. J. Fisher and R. J. Knipe, "Fault sealing processes in siliciclastic sediments," *Geological Society, London, Special Publications*, vol. 147, no. 1, pp. 117–134, 1998.

[13] Q. J. Fisher and R. J. Knipe, "The permeability of faults within siliciclastic petroleum reservoirs of the North Sea and Norwegian continental shelf," *Marine and Petroleum Geology*, vol. 18, no. 10, pp. 1063–1081, 2001.

[14] H. Fossen, R. A. Schultz, Z. K. Shipton, and K. Mair, "Deformation bands in sandstone: a review," *Journal of the Geological Society*, vol. 164, no. 4, pp. 755–769, 2007.

[15] Z. Liu, X. Fu, S. Deng et al., "The critical control of arkosic sandstone porosity on deformation band formation: insights from the Shulu across-fault borehole in the Bohai Bay Basin, China," *Journal of Structural Geology*, vol. 143, article 104258, 2021.

[16] Z. Liu and Y. Sun, "Characteristics and formation process of contractional deformation bands in oil-bearing sandstones in the hinge of a fold: a case study of the Youshashan anticline, western Qaidam basin, China," *Journal of Petroleum Science and Engineering*, vol. 189, article 106994, 2020.

[17] L. D. Meng, *Risk Evaluation for Safety of Hydrocarbon Exploitation and Geologic Storage of Natural Gas in Fault Related Traps*, Northeast Petroleum University, 2016.

[18] S. R. Ogilvie and P. W. Glover, "The petrophysical properties of deformation bands in relation to their microstructure," *Earth and Planetary Science Letters*, vol. 193, no. 1-2, pp. 129–142, 2001.

[19] G. C. Rawling, L. B. Goodwin, and J. L. Wilson, "Internal architecture, permeability structure, and hydrologic significance of contrasting fault-zone types," *Geology*, vol. 29, no. 1, p. 43, 2001.

[20] H. Fossen, L. F. Zuluaga, G. Ballas, R. Soliva, and A. Rotevatn, "Contractional deformation of porous sandstone: insights from the Aztec Sandstone, SE Nevada, USA," *Journal of Structural Geology*, vol. 74, pp. 172–184, 2015.

[21] H. Fossen, R. Soliva, G. Ballas, B. Trzaskos, C. Cavalcante, and R. A. Schultz, "A review of deformation bands in reservoir sandstones: geometries, mechanisms and distribution," *Geological Society, London, Special Publications*, vol. 459, no. 1, pp. 9–33, 2018.

[22] J. G. Solum, J. P. Brandenburg, S. J. Naruk, O. V. Kostenko, S. J. Wilkins, and R. A. Schultz, "Characterization of deformation bands associated with normal and reverse stress States in the Navajo Sandstone, Utah," vol. 94, AAPG Bulletin, 2010.

[23] L. F. Zuluaga, H. Fossen, G. Ballas, and A. Rotevatn, "Structural and petrophysical effects of overthrusting on highly porous sandstones: the Aztec Sandstone in the Buffington window, SE Nevada, USA," *Geological Society, London, Special Publications*, vol. 459, 2018.

[24] H. Fossen and A. Bale, "Deformation bands and their influence on fluid flow," *AAPG Bulletin*, vol. 91, no. 12, pp. 1685–1700, 2007.

[25] D. Kolyukhin, S. Schueller, M. S. Espedal, and H. Fossen, "Deformation band populations in fault damage zone—impact on fluid flow," *Computational Geosciences*, vol. 14, no. 2, pp. 231–248, 2010.

[26] A. Torabi, H. Fossen, and A. Braathen, "Insight into petrophysical properties of deformed sandstone reservoirs," *AAPG Bulletin*, vol. 97, no. 4, pp. 619–637, 2013.

[27] C. Tueckmantel, Q. J. Fisher, C. A. Grattoni, and A. C. Aplin, "Single- and two-phase fluid flow properties of cataclastic fault rocks in porous sandstone," *Marine and Petroleum Geology*, vol. 29, no. 1, pp. 129–142, 2012.

[28] Z. K. Shipton, J. P. Evans, and L. B. Thompson, "The geometry and thickness of deformation-band fault core and its influence on sealing characteristics of deformation-band fault zones, and petroleum traps," *AAPG Memoir*, vol. 85, pp. 181–195, 2005.

[29] T. R. Harper and E. R. Lundin, "Fault seal analysis: reducing our dependence on empiricism," in *Norwegian Petroleum Society Special Publications*, pp. 149–164, Elsevier, 1997.

[30] R. G. Gibson, "Physical character and fluid-flow properties of sandstone-derived fault zones," *Geological Society, London, Special Publications*, vol. 127, no. 1, pp. 83–97, 1998.

[31] J. P. Brandenburg, F. O. Alpak, J. G. Solum, and S. J. Naruk, "A kinematic trishear model to predict deformation bands in a fault-propagation fold, East Kaibab monocline, Utah," *AAPG Bulletin*, vol. 96, no. 1, pp. 109–132, 2012.

[32] M. Pizzati, F. Balsamo, and F. Storti, "Displacement-dependent microstructural and petrophysical properties of deformation bands and gouges in poorly lithified sandstone deformed at shallow burial depth (Crotone Basin, Italy)," *Journal of Structural Geology*, vol. 137, article 104069, 2020.

[33] H. Jourde, E. A. Flodin, A. Aydin, L. J. Durlofsky, and X. Wen, "Computing permeability of fault zones in eolian sandstone from outcrop measurements," *AAPG Bulletin*, vol. 86, 2002.

[34] B. R. Crawford, "Experimental fault sealing: shear band permeability dependency on cataclastic fault gouge characteristics," *Geological Society, London, Special Publications*, vol. 127, no. 1, pp. 27–47, 1998.

[35] F. Balsamo, F. Storti, and D. R. Gröcke, "Fault-related fluid flow history in shallow marine sediments from carbonate concretions, Crotone basin, south Italy," *Journal of the Geological Society*, vol. 169, no. 5, pp. 613–626, 2012.

[36] Z. K. Shipton, J. P. Evans, K. R. Robeson, C. B. Forster, and S. Snelgrove, "Structural heterogeneity and permeability in faulted eolian sandstone: implications for subsurface modeling of faults," *AAPG Bulletin*, vol. 86, pp. 863–883, 2002.

[37] T. Yong, L. Keji, W. Jieming et al., "Change of phase state during multi-cycle injection and production process of condensate gas reservoir based underground gas storage," *Petroleum Exploration and Development*, vol. 48, no. 2, pp. 395–406, 2021.

[38] L. D. Meng, X. F. Fu, X. L. Zhang, T. W. Li, and J. Liu, "Assessment of fault-seal integrity for underground storage of natural gas in porous sandstone," *Fourth International Conference on Fault and Top Seals*, 2015, pp. 1–5, Alméria, Spain, 2015.

[39] L. Meng, X. Fu, Y. Lv et al., "Risking fault reactivation induced by gas injection into depleted reservoirs based on the heterogeneity of geomechanical properties of fault zones," *Petroleum Geoscience*, vol. 23, no. 1, pp. 29–38, 2017.

[40] X. Chen, Y. Li, Y. Jiang, Y. Liu, and T. Zhang, "Theoretical research on gas seepage in the formations surrounding bedded gas storage salt cavern," *Petroleum Science*, 2022.

[41] P. Bretan, G. Yielding, and H. Jones, "Using calibrated shale gouge ratio to estimate hydrocarbon column heights," *AAPG Bulletin*, vol. 87, no. 3, pp. 397–413, 2003.

[42] G. Yielding, "Shale gouge ratio – calibration by geohistory," *Norwegian Petroleum Society Special Publications*, vol. 11, pp. 1–15, 2002.

[43] A. Hildenbrand, S. Schlömer, B. M. Krooss, and R. Littke, "Gas breakthrough experiments on pelitic rocks: comparative study with N2, CO2 and CH4," *Geofluids*, vol. 4, no. 1, 2004.

[44] M. Lommatzsch, U. Exner, S. Gier, and B. Grasemann, "Structural and chemical controls of deformation bands on fluid flow: interplay between cataclasis and diagenetic alteration," *AAPG Bulletin*, vol. 99, no. 4, pp. 689–710, 2015.

[45] C. A. J. Wibberley, J. Gonzalez-Dunia, and O. Billon, "Faults as barriers or channels to production-related flow: insights from case studies," *Petroleum Geoscience*, vol. 23, no. 1, pp. 134–147, 2017.

[46] C. Beal, "The viscosity of air, water, natural gas, crude oil and its associated gases at oil field temperatures and pressures," *Transactions of the AIME*, vol. 165, no. 1, pp. 94–115, 1946.

[47] A. L. Lee, M. H. Gonzalez, and B. E. Eakin, "The viscosity of natural gases," *Journal of Petroleum Technology*, vol. 18, no. 8, pp. 997–1000, 1966.

[48] E. Bastesen and A. Braathen, "Extensional faults in fine grained carbonates - analysis of fault core lithology and thickness-displacement relationships," *Journal of Structural Geology*, vol. 32, no. 11, pp. 1609–1628, 2010.

[49] C. Childs, T. Manzocchi, J. J. Walsh, C. G. Bonson, A. Nicol, and M. P. J. Schöpfer, "A geometric model of fault zone and fault rock thickness variations," *Journal of Structural Geology*, vol. 31, no. 2, pp. 117–127, 2009.

[50] Z. K. Shipton, A. M. Soden, J. D. Kirkpatrick, A. M. Bright, and R. J. Lunn, "How thick is a fault? Fault displacement-thickness scaling revisited," in *Earthquakes: Radiated Energy and the Physics of Faulting*, pp. 193–198, Geophysical Monograph Series 170, 2006.

[51] A. Torabi and S. S. Berg, "Scaling of fault attributes: a review," *Marine and Petroleum Geology*, vol. 28, no. 8, pp. 1444–1460, 2011.

[52] C. A. J. Wibberley, G. Yielding, and G. Di Toro, "Recent advances in the understanding of fault zone internal structure: a review," *Geological Society, London, Special Publications*, vol. 299, no. 1, pp. 5–33, 2008.

[53] H. Fossen, *Structural Geology*, Cambridge University Press, 2012.

[54] D. Brantley, M. Waddell, J. Shafer, and V. Lakshmi, "Inclusion of faults in 3-D numerical simulation of carbon dioxide injection into the South Georgia Rift Basin, South Carolina," *International Journal of Earth Science and Geophysics*, vol. 2, no. 1, 2016.